

Article

# Depositional Environment and Organic Matter Enrichment in the Lower Paleozoic Shale from the Northeastern Margin of the Yangtze Platform, South China

Peng Liu <sup>1</sup>, Changjie Liu <sup>2,\*</sup> and Ruiliang Guo <sup>3,\*</sup>

<sup>1</sup> College of Safety Science and Engineering, Xi'an University of Science and Technology, Xi'an 710054, China

<sup>2</sup> Northwest Institute of Eco-Environment and Resources, Chinese Academy of Sciences, Key Laboratory of Petroleum Resources, Lanzhou 730000, China

<sup>3</sup> School of Earth Sciences and Engineering, Xi'an Shiyou University, Xi'an 710065, China

\* Correspondence: liuchangjie@nieer.ac.cn (C.L.); 210106@xsyu.edu.cn (R.G.)

**Abstract:** In this study, twenty-six core shale samples were collected from the marine Lower Paleozoic shale in a well in the northeastern margin of the Yangtze Platform. Analyses of TOC content, mineral composition, major elements, along with trace and rare earth elements were conducted on the samples. The results were used to investigate the depositional conditions and their effects on organic matter accumulation and preservation. Generally, the sedimentation period of Niutitang Formation shale was in a cold and arid climate with anoxic marine environments, while the shale from Wufeng-Longmaxi Formation was formed in a warm and humid climate with oxic marine environments. In addition, the Wufeng-Longmaxi and Niutitang formations are characterized by low paleo-productivity. The organic matter enrichment for shale in this study could be simultaneously controlled by paleo-redox state and paleo-productivity. Organic matter enrichment of the Niutitang shale is mainly driven by preservation rather than productivity, while the dominant driving factor is the opposite for the Wufeng-Longmaxi shale. Additionally, palaeoclimate and terrestrial influx intensity were found to significantly impact the organic matter enrichment in the Wufeng-Longmaxi shale. The findings have implications for the understanding of the sedimentary processes, organic matter enrichment and preservation and shale gas potential of the study area.

**Keywords:** Yangtze Platform; Lower Paleozoic; black shale; depositional condition; organic matter



**Citation:** Liu, P.; Liu, C.; Guo, R. Depositional Environment and Organic Matter Enrichment in the Lower Paleozoic Shale from the Northeastern Margin of the Yangtze Platform, South China. *J. Mar. Sci. Eng.* **2023**, *11*, 501. <https://doi.org/10.3390/jmse11030501>

Academic Editors: George Kontakiotis, Assimina Antonarakou and Dmitry A. Ruban

Received: 22 January 2023

Revised: 17 February 2023

Accepted: 20 February 2023

Published: 25 February 2023



**Copyright:** © 2023 by the authors. Licensee MDPI, Basel, Switzerland. This article is an open access article distributed under the terms and conditions of the Creative Commons Attribution (CC BY) license (<https://creativecommons.org/licenses/by/4.0/>).

## 1. Introduction

Shale gas is an important unconventional natural gas resource that has gained worldwide attention, and the marine shale gas in the Sichuan Basin of China has been the subject of significant breakthroughs in recent years [1–3]. Additionally, the widely developed and distributed Lower Paleozoic black shale near the Micangshan-Hannan Uplift in the northeastern margin of the Yangtze Platform, which is adjacent to the north Sichuan Basin, is considered to have shale gas potential due to its high TOC content, thickness, and maturity level [4]. However, studies of the Lower Paleozoic shale in the northeastern margin of the Yangtze Platform are still limited compared to that in the Sichuan Basin.

Unlike natural gas from conventional (e.g., sandstone) reservoirs, shale gas is generated and preserved within the source rock [5]. The organic matter in shale can contribute to the generation of hydrocarbons via thermal decomposition processes as the precursors of petroleum and natural gas [6]. Studies have shown that the adsorption capacity of marine shale is positively correlated with its total organic carbon (TOC) content due to the organic pores in the shale matrix [7–9]. As a result, the organic matter in marine shale could have a considerable impact on hydrocarbon generation as well as the occurrence of gas hydrocarbons in shale. Depositional conditions, such as paleo-productivity, preservation conditions (e.g., redox conditions, paleo-water depth), terrestrial influx, and paleo-salinity, can all

impact the accumulation and preservation of organic matter in sediments [10–13]. Depositional conditions can undoubtedly affect the accumulation and dispersion of elements in sediments [14]. Hence, inorganic geochemical proxies, including specific element abundances and ratios, have been applied to infer paleo depositional conditions for sediments and indicate the enrichment and preservation of organic matter [15–17]. However, specific paleo-environmental geochemical proxies show weather-related alteration in outcrop samples [18], suggesting that drilling core samples could better record the paleo-environmental characteristics. In a previous study, Liu et al., (2021) studied the organic matter accumulation of the Niutitang Formation in the SND-1 Well in the northeastern margin of the Yangtze Platform [19]. However, the depositional environment and organic matter enrichment of the shale in the Lower Paleozoic strata of the northeastern margin of the Yangtze Platform, mainly including the Wufeng-Longmaxi shale and Niutitang shale, have yet to be extensively studied through core samples.

Hence, core shale samples were collected from a well in the northeastern margin of the Yangtze Platform in this study, consisting of Wufeng-Longmaxi shale samples and Niutitang shale samples. The TOC content, mineral composition, major elements, trace elements and rare earth elements analyses were conducted to investigate the depositional conditions and their impacts on the accumulation and preservation of organic matter. The results of this study contribute to an improved understanding of the depositional conditions and their effects on the enrichment of organic matter in the Lower Paleozoic shale in the northwestern margin of the Yangtze Platform.

## 2. Geological Setting

The Micangshan-Hannan Uplift is located in the northwestern margin of the Yangtze Platform and acted as the coupling unit of the South Qinling Dabie orogenic belt and Sichuan Basin [20–22]. The Micangshan-Hannan Uplift is adjacent to the Mianlue suture zone to the north, the Sichuan Basin to the south, the Bikou block to the northwest, the Longmenshan Tectonic Zone to the southeast, the Dabashan Folding Belt to the east (Figure 1) [23].

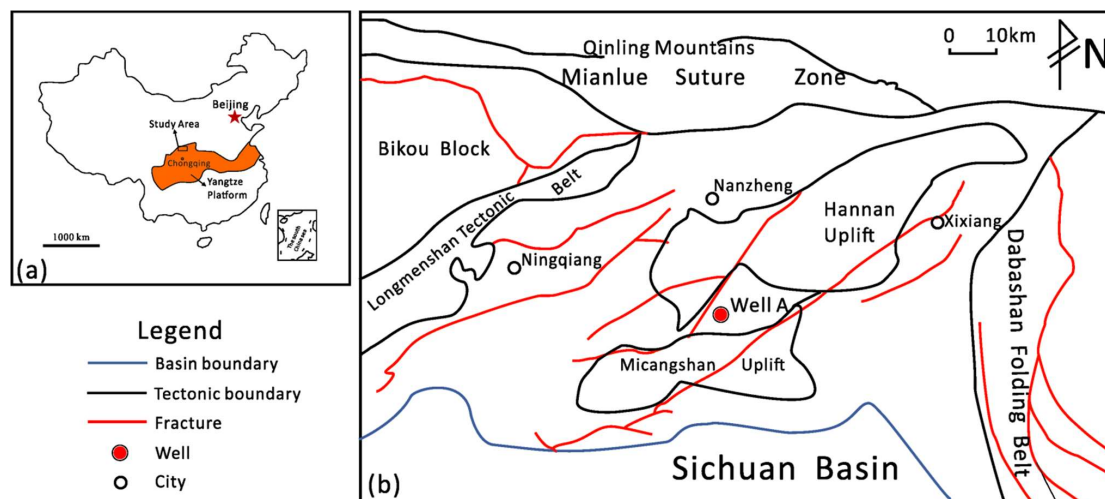


**Figure 1.** Location of the study area in the Yangtze Platform (a) and the geological map of the study area in the northern part of the Yangtze Platform and well location (b). The geological map of the study area is modified from Chen et al., (2019) [21].

The Yangtze Platform was developed on the Precambrian basement [24]. During the Jinning movement, the Micangshan area evolved from a continental margin basin to a back-arc basin. The ancient Qinling Ocean was formed in the early Jinning period and the ancient Qinling Oceanic block was subducted under the Yangtze Platform, forming the arc-basin system [25]. In the Early Sinian, the west and north margin of the Yangtze

Platform was a stretched state and eventually formed the Longmenshan-Micangshan continental rift belt [25]. The Micangshan-Hannan Uplift was the result of continuous collision and subduction of the Yangtze Plate and the North China Plate, and it was uplifted from the Late Triassic [26]. The Micangshan area formed the present geological structural characteristics in the Late Himalayan period. With the increasing sea level in the Early Cambrian, the Niutitang shale was widely distributed in the Sichuan Basin and its adjacent areas, including Micangshan area [27,28]. The shale is of relatively high maturity level and high TOC contents [29]. The Silurian Wufeng-Longmaxi formations were also widely deposited and distributed in the Sichuan basin and its adjacent areas [30]. However, a regional uplift occurred in the north margin area of the Yangtze Platform and the termination period of the uplift varied in different areas, which led to different depositional characteristics of the Ordovician-Silurian strata in Micangshan area [31].

### 3. Samples and Analyses

#### 3.1. Samples

The stratigraphic sequences of the Wufeng-Longmaxi and the Niutitang Formations in Well A are shown in Figure 2. The location of the well in the Huijunba syncline is shown in Figure 1b. 26 core shale samples were collected from this well. Due to the non-continuous drilling and core sampling of this well, only upper and lower samples of the Longmaxi Formation are available. Nine of them were collected from the Wufeng-Longmaxi Formations with depths ranging from 1366.90 m to 1428.21 m. Samples 1 to 4 were collected from the upper part of the Longmaxi Formation, samples 5 to 7 were collected from the lower part of the Longmaxi Formation, and samples 8 and 9 were collected from the Wufeng Formation. Seventeen shale core samples were collected from the Niutitang Formation and the depths range from 2168.93 m to 2384.77 m. The lithology of the collected core samples was shale.

#### 3.2. Analyses

Total organic carbon (TOC), mineral compositions, major elements, and trace and rare earth elements analyses were performed on the core shale samples.

- (1) **TOC analysis:** The shale samples were crushed and ground to greater than 200 mesh. The powdered sample was subjected to hydrochloric acid treatment ( $V_{\text{analytically pure HCl}}: V_{\text{water}} = 1:7$ ) and kept at temperatures between 60 and 80 °C for two hours to thoroughly dissolve the carbonate minerals. The remaining material was dried at 100 °C after being rinsed with distilled water to a neutral pH. Finally, samples were analyzed on the CS-230 Carbon-Sulfur analyzer (LECO). The TOC contents are reported as wt%, after taking into account the material lost by acid treatment. The analytical uncertainty is less than 0.5%.
- (2) **Mineral compositions analysis:** A Bruker D8 Advance X-ray diffractometer with a Cu tube was used to analyze the mineral compositions after the shale had been crushed to more than 200 mesh. The Tube voltage and electric current were  $\leq 40$  kV and  $\leq 40$  mA, respectively. The scan ranges from 0 to 140° with a rate of 2°/min and step size of 0.02°. The analytical uncertainty is less than 5%.
- (3) **Major elements analysis:** The powdered samples (greater than 200 mesh) were dried at 105 °C and compressed into a specimen (32 mm i.d.) under the pressure of 30 tons using boric acid to rim the substrate. Then, the compressed specimen was measured by an Axios Panalytical X-ray fluorescence (XRF) spectrometry to obtain the concentration of the major elements. The analytical uncertainty is less than 3%.
- (4) **Trace and rare earth elements analysis:** Trace and rare earth elements concentration analysis was carried out by inductively coupled plasma mass spectrometry (ICP-MS) (Nu Atom, UK). The powder samples with >200 mesh were dried at 55 °C for 12 h. After that, the powder sample was digested by acid solution ( $\text{HNO}_3 + \text{HF}$ ). Then, the solutions were transferred and diluted for ICP-MS analysis to access the trace and rare earth elements concentration. Generally, the analytical uncertainty for most elements is less than 2%.

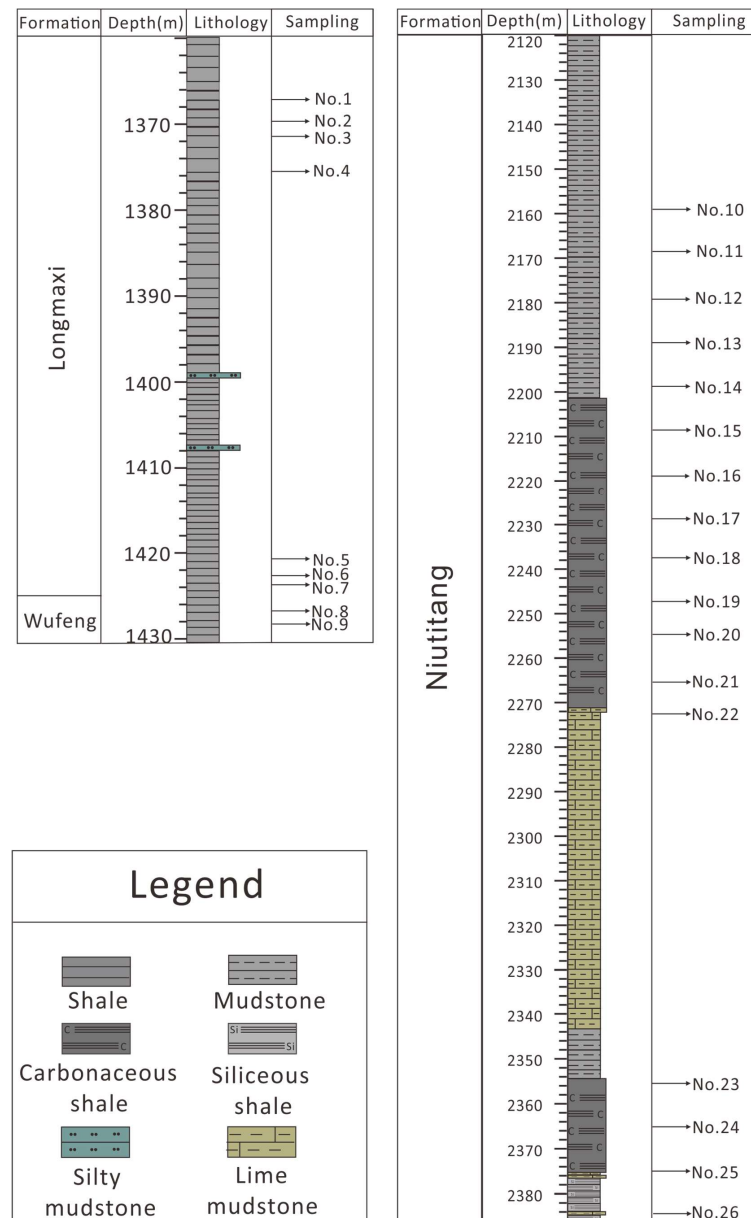


Figure 2. Stratigraphic sequences and the sampling depths of the Wufeng-Longmaxi Formation and the Niutitang Formation.

#### 4. Results

##### 4.1. TOC Content and Mineral Composition

TOC content and mineral composition for shale samples are given in Table 1. The TOC contents of the shale from the Upper part of the Longmaxi Formation, Lower part of the Longmaxi Formation, Wufeng-Longmaxi shale and Niutitang shale range from 0.06% to 0.26%, 1.15% to 1.63%, 1.42% to 2.86% and 0.15% to 2.56%, respectively. The mineral composition characteristics of the Wufeng-Longmaxi shale and Niutitang shale are different. In general, the shale is dominated by quartz, feldspar, and clay but of varying average proportions in different formations. The Wufeng-Longmaxi shale has average proportions of quartz, feldspar, and clay of 38.3%, 12.2%, and 27.9%, respectively. The average proportions for the same major minerals in the Niutitang shale are 29.2%, 31.4%, and 20.8%, respectively.

**Table 1.** TOC contents and mineral compositions of Wufeng-Longmaxi and Niutitang samples.

Formation	Sample Number	Depths (m)	TOC	Mineral Compositions									Total
				Quartz	Feldspar	Berlinite	Muscovite	Pyrite	Clay	Calcite	Dolomite		
				%	%	%	%	%	%	%	%	%	
Wufeng-Longmaxi	1	1366.90	0.08	39.6	9.3	/	11.0	/	40.1	/	/	100.0	
	2	1369.90	0.06	39.6	21.4	6.4	15.6	/	17.0	/	/	100.0	
	3	1371.86	0.09	44.5	13.7	8.4	8.3	/	25.1	/	/	100.0	
	4	1375.60	0.26	29.6	26.7	8.7	15.7	/	19.3	/	/	100.0	
	5	1420.90	1.15	39.8	6.5	/	23.9	/	29.8	/	/	100.0	
	6	1422.75	1.63	33.4	8.6	12.4	18.0	/	27.6	/	/	100.0	
	7	1423.75	1.40	35.3	4.8	8.8	20.5	/	30.6	/	/	100.0	
	8	1426.50	2.86	40.4	6.7	6.5	12.5	/	32.5	/	1.4	100.0	
	9	1428.21	1.42	42.5	12.4	7.5	8.2	/	29.4	/	/	100.0	
Niutitang	10	2158.70	0.97	27.7	24.9	9.1	5.5	1.6	28.3	2.1	0.8	100.0	
	11	2168.93	0.71	35.4	14.4	7.6	18.2	/	22.0	1.2	1.2	100.0	
	12	2179.25	0.66	31.2	22.4	4.6	17.7	/	18.9	4.4	0.8	100.0	
	13	2188.60	0.79	29.3	24.7	4.6	13.9	/	22.9	2.8	1.8	100.0	
	14	2198.00	0.98	32.1	14.9	/	12.5	1.4	34.3	3.3	1.5	100.0	
	15	2208.00	1.97	26.6	36.6	6.0	13.7	/	15.8	1.3	/	100.0	
	16	2218.50	1.58	35.7	22.7	7.8	16.0	/	17.8	/	/	100.0	
	17	2228.84	1.22	24.4	32.0	7.4	10.9	0.8	24.5	/	/	100.0	
	18	2237.38	1.28	36.3	33.2	5.4	6.6	/	18.5	/	/	100.0	
	19	2246.86	0.90	37.2	30.9	7.4	6.0	/	18.5	/	/	100.0	
	20	2254.60	1.10	24.9	27.4	9.4	12.9	1.1	24.3	/	/	100.0	
	21	2265.80	1.18	24.5	39.4	9.5	4.6	1.1	20.9	/	/	100.0	
	22	2273.20	0.15	21.9	49.7	/	3.7	1.0	23.0	/	0.7	100.0	
	23	2355.80	2.56	29.1	48.1	5.4	4.3	/	13.1	/	/	100.0	
	24	2365.66	2.54	25.9	46.9	4.0	11.6	/	11.6	/	/	100.0	
	25	2375.95	1.96	24.4	35.3	8.6	11.6	1.7	18.4	/	/	100.0	
	26	2384.77	1.68	31.3	29.6	10.5	6.2	1.8	20.6	/	/	100.0	

4.2. Major Elements

Major element concentrations of the shale samples are presented in Table 2. No significant difference in major element oxide distribution can be observed between the Wufeng-Longmaxi and the Niutitang samples. The dominant major element oxides are SiO<sub>2</sub>, Al<sub>2</sub>O<sub>3</sub>, and TFe<sub>2</sub>O<sub>3</sub>. The Wufeng-Longmaxi shale has an average SiO<sub>2</sub> content of 63.96%, with a range of 62.22% to 67.94%, while the SiO<sub>2</sub> abundance in the Niutitang shale ranges from 53.69% to 65.74% with an average of 60.41%. The average Al<sub>2</sub>O<sub>3</sub> and TFe<sub>2</sub>O<sub>3</sub> contents in the Wufeng-Longmaxi shale are 16.14% and 6.32%, respectively, while the Niutitang shale has average Al<sub>2</sub>O<sub>3</sub> and TFe<sub>2</sub>O<sub>3</sub> contents of 13.95% and 5.37%, respectively. Other major element oxides, including CaO, MgO, K<sub>2</sub>O, Na<sub>2</sub>O and P<sub>2</sub>O<sub>5</sub>, are present in relatively low amounts (less than 5%).

**Table 2.** Major elements data of Wufeng-Longmaxi and Niutitang samples.

Formation	Sample Number	Depths (m)	SiO <sub>2</sub> %	Al <sub>2</sub> O <sub>3</sub> %	TFe <sub>2</sub> O <sub>3</sub> %	CaO %	MgO %	K <sub>2</sub> O %	Na <sub>2</sub> O %	P <sub>2</sub> O <sub>5</sub> %	TiO <sub>2</sub> %	MnO %	Other %	Total %
Wufeng-Longmaxi	1	1366.90	63.24	16.68	6.79	0.32	2.30	4.09	1.22	0.11	0.74	0.08	4.12	99.71
	2	1369.90	67.94	14.18	5.54	0.65	2.04	3.14	1.33	0.13	0.73	0.10	3.97	99.75
	3	1371.86	66.18	14.92	6.21	0.44	2.15	3.35	1.31	0.13	0.74	0.08	4.25	99.74
	4	1375.60	67.08	15.38	6.44	0.36	2.21	3.46	1.28	0.12	0.72	0.08	2.59	99.72
	5	1420.90	62.41	17.29	6.43	0.71	2.38	4.50	1.08	0.10	0.70	0.07	3.74	99.39
	6	1422.75	62.22	16.90	6.61	1.13	2.42	4.40	0.98	0.09	0.72	0.07	3.64	99.17
	7	1423.75	65.65	15.88	5.64	0.67	2.21	4.20	1.08	0.10	0.65	0.06	3.22	99.35
	8	1426.50	58.57	16.16	7.83	1.29	2.24	4.09	1.05	0.10	0.79	0.07	5.67	97.84
	9	1428.21	62.38	17.87	5.44	1.02	1.79	4.67	1.00	0.09	0.49	0.04	3.64	98.43
average			63.96	16.14	6.32	0.73	2.19	3.99	1.15	0.11	0.46	0.26	0.26	99.23
Niutitang	10	2158.70	56.22	14.72	6.66	4.79	3.17	3.53	1.24	0.19	0.72	0.09	7.48	98.81
	11	2168.93	55.08	14.56	6.48	5.82	3.27	3.40	1.20	0.21	0.76	0.12	8.01	98.89
	12	2179.25	56.57	14.82	6.07	5.26	3.21	3.49	1.26	0.23	0.78	0.09	7.27	99.05
	13	2188.60	53.69	14.65	6.14	6.82	3.53	3.52	1.16	0.24	0.75	0.12	8.50	99.10
	14	2198.00	54.42	14.61	5.93	6.76	3.41	3.51	1.18	0.24	0.75	0.11	8.21	99.13
	15	2208.00	58.60	13.80	5.58	4.68	2.70	3.13	1.62	0.17	0.75	0.07	7.68	98.79
	16	2218.50	61.13	14.21	5.36	3.02	2.62	3.30	1.61	0.19	0.73	0.06	6.75	98.96
	17	2228.84	63.43	12.52	4.66	3.19	2.24	2.76	1.94	0.21	0.74	0.06	7.37	99.11
	18	2237.38	62.71	14.15	5.07	2.65	2.76	3.21	1.65	0.18	0.75	0.06	6.00	99.19
	19	2246.86	61.92	13.77	5.32	2.73	2.70	3.20	1.62	0.19	0.75	0.06	6.90	99.15
	20	2254.60	62.84	13.92	5.41	2.26	2.61	3.18	1.72	0.19	0.75	0.05	6.12	99.06
	21	2265.80	65.74	12.22	4.77	3.00	2.01	2.64	2.20	0.24	0.71	0.05	5.26	98.85
	22	2273.20	62.88	12.22	4.00	3.74	2.21	2.52	3.03	0.47	0.73	0.05	7.48	99.32
	23	2355.80	62.65	12.79	4.88	1.93	2.10	3.12	1.84	0.22	0.80	0.04	8.44	98.80
	24	2365.66	63.53	12.98	4.74	2.85	2.09	3.00	2.10	0.24	0.81	0.06	6.45	98.85
	25	2375.95	63.03	15.45	5.31	1.53	2.37	3.61	1.93	0.21	0.83	0.04	4.04	98.35
	26	2384.77	62.49	15.83	4.94	2.06	1.92	3.60	1.59	0.25	0.82	0.04	4.58	98.10
average			60.41	13.95	5.37	3.71	2.64	3.22	1.70	0.23	0.76	0.07	6.86	98.91

### 4.3. Trace Elements

The abundances of selected trace elements of the Wufeng-Longmaxi and Niutitang samples in the study area are shown in Table 3. The UCC-normalized trace elements of shale from the Wufeng-Longmaxi Formation and the Niutitang Formation are illustrated in Figure 3. The distribution characteristics of trace elements in the Wufeng-Longmaxi samples are different, as demonstrated by the findings in Figure 3a. Cu, Sr, Mo, and Pb are depleted in the shale samples from 1366.90 m to 1375.60 m (Nos. 1–4). However, Cu, Mo, Pb and U are obviously enriched in samples from 1420.90 m to 1428.21 m (Nos. 5–9). The UCC-normalized trace element distributions of the Niutitang samples show a similar distribution pattern compared to the Wufeng-Longmaxi shale with depths ranging from 1420.90 m to 1428.21 m (Figure 3b). In general, the majority of the samples from the Niutitang samples are enriched in Mo, Cd and U.

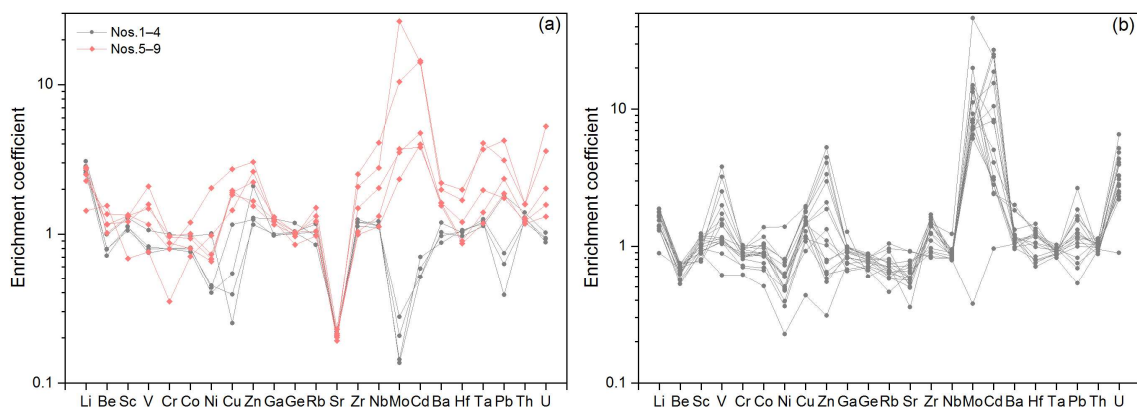


**Figure 3.** UCC-normalized trace element distributions for the Wufeng-Longmaxi shale (a) and the Niutitang shale (b). The enrichment coefficient can be expressed as  $X_{\text{sample}}/X_{\text{UCC}}$ , where X represents the weight concentrations of elements X.

### 4.4. Rare Earth Elements

Rare earth element concentrations of the samples are presented in Table 4 and Figure 4. The average  $\Sigma\text{REE}$  contents of the Wufeng-Longmaxi and the Niutitang samples are 209.93  $\mu\text{g/g}$  and 166.90  $\mu\text{g/g}$ , respectively. The Niutitang and the Wufeng-Longmaxi samples have average light rare earth elements ( $\Sigma\text{LREEs}$ ) of 187.36  $\mu\text{g/g}$  and 146.51  $\mu\text{g/g}$ , respectively. The average heavy rare earth elements ( $\Sigma\text{HREEs}$ ) in the Wufeng-Longmaxi and the Niutitang samples are 22.57  $\mu\text{g/g}$  and 20.38  $\mu\text{g/g}$ , respectively.

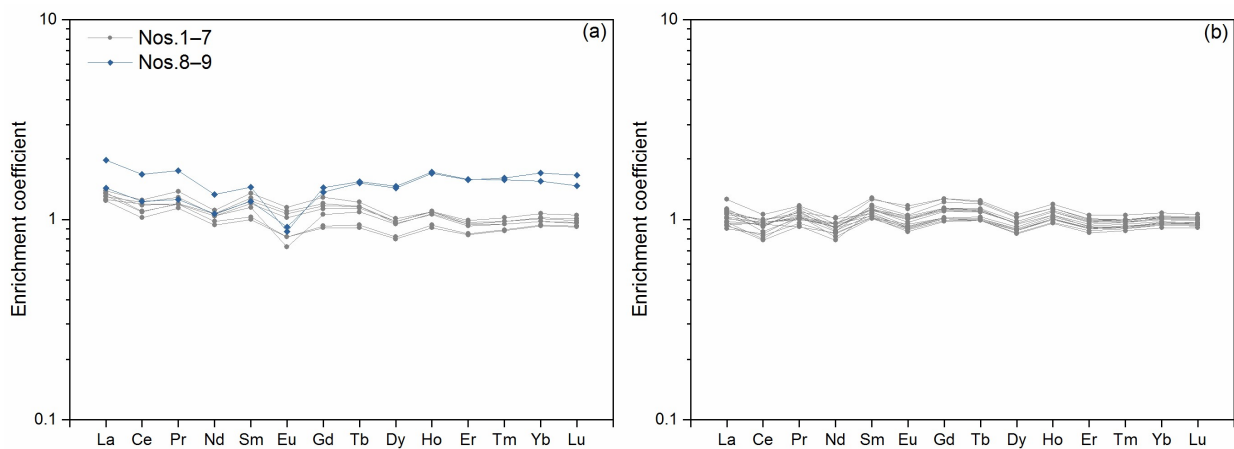


**Figure 4.** NASC —normalized REEs distribution for the samples from the Wufeng-Longmaxi Formations (a) and the Niutitang Formation (b). NASC = The North American shale composite from McLennan (1989) [32]. The enrichment coefficient can be expressed as  $X_{\text{sample}}/X_{\text{NASC}}$ , where X represents the weight concentrations of elements X.

**Table 3.** Trace elements data of Wufeng-Longmaxi and Niutitang samples.

Formation	Sample Number	Depths (m)	Li	Be	Sc	V	Cr	Co	Ni	Cu	Zn	Ga	Ge	Rb	Sr	Zr	Nb	Mo	Cd	Ba	Hf	Ta	Pb	Th	U
			µg/g																						
Wufeng-Longmaxi	1	1366.90	61.40	2.98	17.45	113.39	84.64	16.43	44.29	6.28	91.14	21.51	1.89	109.01	72.91	226.31	14.56	0.20	0.05	655.30	5.95	1.26	12.61	13.44	2.63
	2	1369.90	51.17	2.14	15.27	79.88	67.41	12.92	33.98	13.49	148.59	16.73	1.60	116.26	71.51	237.03	13.60	0.21	0.07	480.08	6.16	1.17	10.67	12.76	2.59
	3	1371.86	53.16	2.38	14.37	84.94	67.81	13.75	36.68	28.86	88.59	16.56	1.64	94.73	76.76	228.66	13.63	0.31	0.06	532.89	6.07	1.20	6.55	13.81	2.46
	4	1375.60	56.71	2.36	15.19	88.15	67.53	13.49	37.91	9.75	82.15	16.93	1.66	130.53	71.36	213.07	13.33	0.41	0.05	563.13	5.61	1.13	30.96	14.87	2.86
	5	1420.90	54.87	3.04	17.81	223.38	81.40	15.87	57.71	48.92	109.31	19.63	1.60	147.25	72.75	188.34	13.41	3.49	0.39	852.31	5.01	1.18	31.68	12.51	3.67
	6	1422.75	55.91	3.48	18.04	158.22	82.48	17.04	62.26	45.76	118.28	21.11	1.64	136.39	74.56	196.92	15.84	5.57	0.37	884.21	5.20	1.39	39.97	13.67	5.64
	7	1423.75	50.17	3.50	16.46	169.05	73.82	13.64	55.76	47.26	157.69	22.05	1.65	117.23	67.15	283.33	24.47	5.29	0.46	894.24	6.97	1.96	29.60	13.03	4.39
	8	1426.50	45.48	4.07	18.29	123.72	67.38	20.34	173.12	67.93	216.24	21.12	1.54	168.28	79.86	392.94	33.33	39.84	1.38	1089.65	9.79	4.06	52.88	16.99	14.74
	9	1428.21	28.70	4.66	9.32	81.46	29.63	12.03	83.17	36.09	186.41	20.76	1.35	108.56	70.68	478.97	49.12	15.65	1.41	1210.13	11.46	3.70	71.91	16.91	10.04
Niutitang	10	2158.70	37.45	2.24	13.85	211.89	81.58	19.90	64.61	47.53	314.88	16.49	1.38	72.27	231.66	170.23	9.70	12.42	2.65	614.29	4.56	0.87	44.95	9.80	8.59
	11	2168.93	37.56	2.11	13.89	269.18	81.63	17.47	67.41	44.35	287.45	16.42	1.35	65.58	271.11	173.93	10.16	11.93	2.44	539.22	4.63	0.88	31.38	9.85	7.93
	12	2179.25	37.27	2.22	12.29	342.91	86.53	17.03	68.38	45.01	238.01	16.90	1.41	82.91	274.90	183.65	10.77	9.78	1.83	668.00	4.86	0.94	26.27	9.77	7.69
	13	2188.60	33.02	2.24	10.52	155.66	71.24	14.74	50.17	36.64	148.43	15.58	1.32	117.19	318.98	160.62	9.84	11.13	1.03	667.63	4.39	0.89	22.39	10.19	7.72
	14	2198.00	35.15	2.08	10.90	184.15	73.09	15.24	61.53	38.61	211.33	16.92	1.33	107.88	322.79	156.54	9.68	16.81	1.51	631.54	4.11	0.85	19.43	9.35	9.14
	15	2208.00	32.65	1.95	14.08	122.95	68.34	17.82	40.56	38.32	46.10	14.24	1.21	79.39	253.23	233.45	10.07	22.47	0.31	545.17	6.10	0.90	28.14	11.10	11.04
	16	2218.50	33.55	2.11	13.40	119.10	71.29	15.29	39.72	35.98	78.17	13.92	1.26	79.24	204.75	209.37	10.39	13.91	0.50	653.60	5.72	0.94	20.73	11.02	9.17
	17	2228.84	30.83	1.71	13.09	94.50	61.08	11.78	30.66	27.01	44.36	11.49	1.14	70.68	203.72	266.21	10.27	9.18	0.30	610.31	7.00	0.91	17.91	10.90	6.16
	18	2237.38	35.18	2.03	12.49	116.63	68.64	12.76	33.34	28.38	72.05	12.67	1.25	65.85	174.23	264.79	10.60	12.56	0.27	526.23	7.09	1.02	12.75	10.58	7.01
	19	2246.86	37.23	1.99	16.11	166.77	76.01	14.33	53.32	36.64	132.33	15.81	1.35	86.13	203.01	236.76	11.16	10.71	0.81	626.99	6.13	0.97	11.72	12.15	6.44
	20	2254.60	35.81	1.91	15.67	151.43	80.99	15.06	42.65	40.45	54.40	16.76	1.35	74.83	186.09	272.48	11.34	10.84	0.27	603.84	6.75	0.96	19.94	11.20	6.82
	21	2265.80	26.05	1.58	12.60	114.38	59.39	11.31	41.41	23.05	94.09	11.15	1.12	64.35	196.47	324.33	9.73	22.46	0.79	727.90	8.46	0.86	16.94	10.51	11.46
	22	2273.20	26.06	1.67	12.03	65.48	52.30	8.57	19.29	10.83	21.88	12.89	1.07	51.24	224.14	281.72	9.49	0.56	0.09	574.39	7.32	0.82	9.03	10.15	2.50
	23	2355.80	27.76	1.86	15.18	111.23	76.39	15.35	50.48	32.03	38.50	15.17	1.29	90.41	205.50	296.12	10.51	29.87	0.24	1004.28	7.57	0.92	19.20	12.20	13.49
	24	2365.66	28.29	1.88	15.78	119.70	72.30	15.08	51.04	29.57	56.47	15.65	1.26	71.96	244.04	308.91	10.87	21.12	0.40	1006.17	7.76	0.96	14.02	11.97	14.56
	25	2375.95	26.69	2.25	16.20	124.07	83.55	16.43	50.78	38.34	40.94	14.24	1.11	102.50	172.50	270.43	11.17	20.08	0.24	1101.38	7.06	0.97	21.13	10.91	12.17
	26	2384.77	17.83	2.05	16.82	407.74	80.86	23.34	117.94	49.02	372.50	21.61	0.96	79.66	124.23	280.09	14.71	69.21	2.36	578.59	7.11	0.92	26.99	11.80	18.26
UCC *			20.00	3	13.6	107	85	17	44	25	71	17	1.6	112	350	190	12	1.5	0.098	550	5.8	1	17	10.7	2.8

\* The UCC data was from Taylor and McLennan (1985) [33] and McLennan et al. (1995) [34].

**Table 4.** Rare earth elements abundances of Wufeng-Longmaxi and Niutitang samples.

Formations	Sample Number	Depth (m)	La	Ce	Pr	Nd	Sm	Eu	Gd	Tb	Dy	Ho	Er	Tm	Yb	Lu	ΣREE
			μg/g														
Wufeng-Longmaxi	1	1366.90	40.41	86.92	9.41	34.30	6.82	1.27	5.86	0.97	5.69	1.15	3.37	0.51	3.30	0.50	200.48
	2	1369.90	42.05	79.59	9.49	35.15	7.29	1.36	6.22	0.98	5.59	1.10	3.16	0.48	3.04	0.46	195.96
	3	1371.86	41.71	88.73	10.16	34.98	7.08	1.32	6.11	0.98	5.70	1.13	3.29	0.49	3.13	0.48	205.30
	4	1375.60	44.56	91.18	10.87	36.57	7.72	1.42	6.68	1.04	5.84	1.14	3.25	0.48	3.05	0.46	214.25
	5	1420.90	39.70	74.75	9.03	31.05	5.70	1.02	4.71	0.77	4.63	0.95	2.85	0.44	2.87	0.44	178.93
	6	1422.75	43.42	80.58	9.37	32.46	5.87	1.02	4.85	0.80	4.77	0.97	2.91	0.45	2.91	0.44	190.82
	7	1423.75	42.73	86.04	9.41	34.24	6.54	0.90	5.49	0.93	5.49	1.11	3.23	0.49	3.18	0.49	200.25
	8	1426.50	45.92	90.08	9.96	35.45	7.02	1.15	7.13	1.29	8.31	1.75	5.32	0.81	5.27	0.80	220.27
	9	1428.21	62.97	122.46	13.81	43.84	8.28	1.08	7.47	1.31	8.45	1.79	5.37	0.79	4.79	0.71	283.11
Niutitang	10	2158.70	31.27	69.06	8.21	30.15	6.61	1.26	5.88	0.94	5.58	1.13	3.32	0.50	3.19	0.49	167.59
	11	2168.93	30.01	71.13	7.87	31.30	7.20	1.45	6.60	1.05	6.16	1.24	3.57	0.53	3.34	0.51	171.97
	12	2179.25	32.48	71.16	8.00	30.23	6.37	1.29	5.93	0.96	5.69	1.16	3.38	0.50	3.21	0.49	170.82
	13	2188.60	33.84	73.22	8.51	30.15	6.37	1.24	5.80	0.94	5.57	1.13	3.32	0.49	3.10	0.48	174.14
	14	2198.00	30.70	69.19	7.30	28.34	5.83	1.18	5.31	0.86	5.14	1.05	3.06	0.46	2.92	0.45	161.80
	15	2208.00	35.40	71.33	9.12	31.43	5.93	1.11	5.24	0.85	5.11	1.04	3.08	0.46	2.97	0.46	173.54
	16	2218.50	32.64	68.22	8.73	28.96	5.97	1.14	5.28	0.86	5.22	1.07	3.16	0.47	3.02	0.46	165.22
	17	2228.84	30.01	57.51	7.36	26.21	6.34	1.24	5.95	0.95	5.51	1.09	3.14	0.46	2.93	0.45	149.15
	18	2237.38	28.78	61.94	8.19	27.18	5.74	1.10	5.14	0.84	5.09	1.04	3.09	0.46	2.97	0.46	152.02
	19	2246.86	34.72	72.77	8.29	31.22	6.43	1.25	5.81	0.95	5.59	1.13	3.29	0.49	3.13	0.48	175.56
	20	2254.60	32.90	70.59	8.05	30.39	6.21	1.15	5.30	0.88	5.31	1.09	3.24	0.49	3.17	0.49	169.27
	21	2265.80	31.18	58.75	8.11	28.80	6.74	1.30	6.34	1.02	5.94	1.18	3.42	0.50	3.22	0.50	157.00
	22	2273.20	29.89	60.36	7.58	28.05	5.83	1.13	5.26	0.84	4.95	1.00	2.91	0.44	2.83	0.44	151.51
	23	2355.80	40.19	77.66	9.26	33.38	6.13	1.13	5.26	0.84	4.99	1.01	2.99	0.45	2.91	0.45	186.63
	24	2365.66	35.17	68.46	8.60	33.68	7.27	1.40	6.59	1.04	5.95	1.18	3.41	0.50	3.21	0.49	176.94
	25	2375.95	36.04	66.93	8.86	29.98	5.80	1.08	5.10	0.84	5.08	1.05	3.10	0.46	3.00	0.47	167.79
	26	2384.77	34.87	63.39	8.09	31.57	6.37	1.20	5.70	0.93	5.55	1.13	3.33	0.50	3.17	0.49	166.29
NASC *			32	73	7.9	33	5.7	1.24	5.2	0.85	5.8	1.04	3.4	0.5	3.1	0.48	/

\* The North American shale composite (NASC) is from McLennan (1989) [32].

The NASC normalized REE distributions of the Wufeng-Longmaxi samples suggest a relative enrichment of LREE. Samples 8 and 9 from the Wufeng Formation have a considerably enriched HREE content. The shale samples from the Niutitang Formation do not show any notable enrichment or depletion of REE compared to NASC (Figure 4).

## 5. Discussion

### 5.1. Chemical Weathering and Palaeoclimate

The palaeoclimate during sedimentation can be reflected by the chemical index of alteration (CIA), which indicates the degree of weathering [35]. The CIA is calculated as follows:

$$CIA(\%) = 100 \times Al_2O_3 / (Al_2O_3 + CaO^* + Na_2O + K_2O) \tag{1}$$

CaO\* stands for calcium that is presented as the silicate. In this study, the CaO\* was calibrated and the CIA (%) was estimated using the method proposed by McLennan (1993) [36]. Chemical weathering is beginning to occur, as indicated by the CIA (%) value range of 50 to 60. CIA (%) values of 60–80 and >80 indicate moderate chemical weathering and strong chemical weathering, respectively [35,37]. CIA (%) in the Wufeng-Longmaxi samples range from 67.27 to 70.37 with an average of 68.62, while the average CIA (%) in the Niutitang samples is 60.25 (Table 5). Chemical alterations become weaker under arid conditions [38]. Therefore, the Wufeng-Longmaxi shale was deposited in warmer and more humid conditions compared to Niutitang shale. However, with decreasing depth, the CIA (%) for the Niutitang shale rises from about 60 to 65, indicating a change in the palaeoclimate conditions.

### 5.2. Terrestrial Influx Intensity, Provenance, and Tectonic Setting

Influx of terrestrial materials can dilute the organic matter and thereby affect its accumulation. The Mn/Ca ratio serves as a proxy for the terrestrial influx intensity [39,40]. Figure 5a demonstrates a cross-plot of Mn/Ca (ppm/%) and Ca (%), which shows variations in terrestrial influx intensity among the samples from different formations. Generally, the Niutitang samples have the lowest terrestrial influx intensity among the shale, while the highest intensity is observed in the shale from the upper of the Longmaxi Formation. The

TiO<sub>2</sub>/Zr ratio can be used to classify the origin of the clastic input to sediment [41], and the results of plotting TiO<sub>2</sub> and Zr suggest a provenance of felsic igneous rock (Figure 5b). Plotting La/Yb versus ΣREE can also be applied to classify the provenance of the sedimentary rocks as REEs inherit the characteristics of parental rocks [32,42,43]. The results of plotting La/Yb versus ΣREE are consistent with the interpretation of the TiO<sub>2</sub>/Zr crossplot and indicate a mixed provenance of granite, sedimentary rock, and alkalic basalts (Figure 5c). The shale from various formations reflects distinct tectonic settings. The majority of the Wufeng-Longmaxi samples are located within the passive margin, whereas the Niutitang samples are mostly located within the active continental margin (Figure 5d).

**Table 5.** Geochemical proxies of the Wufeng-Longmaxi and Niutitang samples.

Formations	Sample Number	Depths (m)	Palaeoclimate	Terrestrial Influx	Paleoredox Conditions			Paleo-Productivity	
			CIA	Mn/Ca (ppm/%)	Th/U	δU	Mo <sub>EF</sub>	U <sub>EF</sub>	P/Ti
Wufeng-Longmaxi	1	1366.90	70.37	2650.03	5.12	0.74	0.23	0.96	0.11
	2	1369.90	67.70	1668.85	4.92	0.76	0.29	1.11	0.13
	3	1371.86	69.37	1920.55	5.62	0.70	0.39	1.00	0.13
	4	1375.60	70.28	2278.78	5.21	0.73	0.51	1.13	0.12
	5	1420.90	68.57	1118.61	3.41	0.94	3.82	1.29	0.10
	6	1422.75	67.93	716.73	2.42	1.11	6.23	2.04	0.09
	7	1423.75	67.85	985.68	2.97	1.01	6.30	1.68	0.11
	8	1426.50	67.27	573.60	1.15	1.44	46.58	5.56	0.10
	9	1428.21	68.20	465.01	1.68	1.28	16.55	3.43	0.13
Niutitang	10	2158.70	65.07	207.62	1.14	1.45	15.94	3.56	0.19
	11	2168.93	65.65	231.71	1.24	1.41	15.49	3.32	0.20
	12	2179.25	65.15	191.60	1.27	1.41	12.47	3.16	0.21
	13	2188.60	65.79	193.14	1.32	1.39	14.36	3.21	0.23
	14	2198.00	65.54	170.65	1.02	1.49	21.75	3.81	0.23
	15	2208.00	61.30	169.88	1.01	1.50	30.77	4.88	0.17
	16	2218.50	61.59	206.73	1.20	1.43	18.50	3.94	0.19
	17	2228.84	57.23	194.78	1.77	1.26	13.86	3.00	0.21
	18	2237.38	61.39	256.56	1.51	1.33	16.79	3.02	0.17
	19	2246.86	61.07	243.33	1.89	1.23	14.70	2.85	0.18
	20	2254.60	60.42	255.42	1.64	1.29	14.73	2.99	0.18
	21	2265.80	54.72	189.00	0.92	1.53	34.76	5.72	0.24
	22	2273.20	49.06	152.62	4.06	0.85	0.87	1.25	0.47
	23	2355.80	56.38	230.11	0.90	1.54	44.14	6.43	0.20
	24	2365.66	52.19	217.88	0.82	1.57	30.77	6.84	0.21
	25	2375.95	61.04	314.68	0.90	1.54	24.57	4.80	0.19
	26	2384.77	60.72	207.92	0.65	1.65	82.62	7.03	0.22

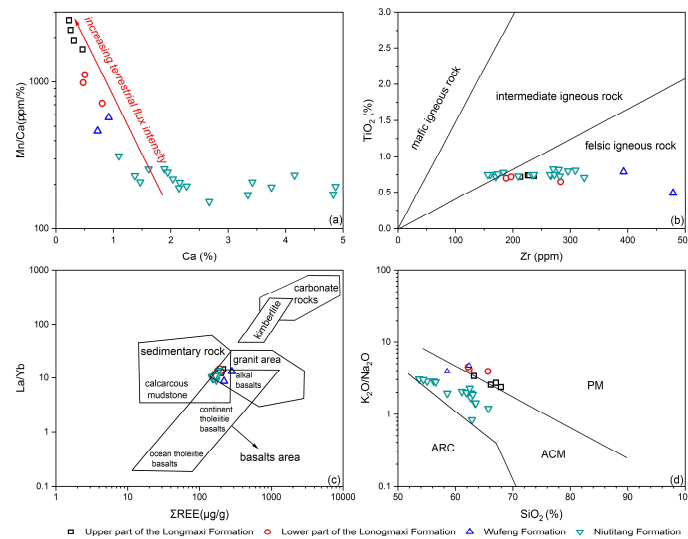


**Figure 5.** (a) Mn/Ca (ppm/%) versus Ca (%) for samples from different formations. (b) TiO<sub>2</sub> versus Zr for samples from different formations. The interpretation lines are from Hayashi et al., (1997) [41]. (c) La/Yb versus ΣREE for samples from different formations. The interpretation lines are from Zhao (2016) [44]. (d) K<sub>2</sub>O/Na<sub>2</sub>O versus SiO<sub>2</sub> for samples from different formations. The interpretation lines are from Roser and Korsch (1986) [45]. ARC: oceanic island arc margin; ACM: active continental margin; PM: passive margin.

### 5.3. Paleoredox Conditions and Water Mass Restriction

Specific ratios for redox-sensitive elements, such as V, Cr, Ni, Co, Mo and U, were employed as redox indicators to evaluate the paleo-redox conditions during sediment deposition [46–49]. In an oxidizing seawater environment, uranium (U) is presented as dissolved U (VI); however, it can be reduced to solid U (IV) and accumulate in sediments under anoxic conditions [14]. In contrast, thorium (Th) is a very stable element that may remain in sediments as undissolved thorium (IV) [47]. Thus, redox conditions may be revealed using the Th/U ratio. Th/U ratios of 2–7 typically indicate oxic marine environments, whereas a ratio of <2 reflects anoxic environments [50,51]. In addition, the Th/U ratio may exceed 7 in a terrestrial oxic environment [51]. Additionally, the paleo-redox conditions can be categorized using the  $\delta U$  value ( $2U/(U + 1/3Th)$ ) [49]. A  $\delta U$  value of >1 suggests anoxic conditions, whereas a value of <1 denotes an oxic environment.

Table 5 presents the Th/U and  $\delta U$  ratios for the samples. The data for the Niutitang samples suggest a mainly anoxic environment, as indicated by Th/U ratios that vary from 0.64 to 4.06, with an average of 1.37. Shale from the Wufeng Formation have a Th/U ratio that varies from 1.15 to 1.68 with an average of 1.42. Samples 5–7 from the Lower Longmaxi Formation have Th/U ratios that vary from 2.42 to 3.41 with an average of 2.93, while the Longmaxi samples 1–4 are characterized by high Th/U with an average of 5.21 (Table 5). These results suggest that the upper Longmaxi samples were deposited in more oxic conditions than the samples from the lower Longmaxi Formation, while the conditions for the Wufeng samples were more anoxic, and similar to the Niutitang Formation during the Wufeng and Longmaxi sedimentary periods. The redox condition interpreted by  $\delta U$  is consistent with Th/U ratios. Most Niutitang, Wufeng, and Longmaxi samples (Nos. 5–7) display  $\delta U$  values greater than 1, indicating anoxic water conditions. The samples 1–4 from the Longmaxi Formation have low  $\delta U$  with an average of 0.73, suggesting oxic water conditions.

Molybdenum (Mo) can exist in sea water as a stable and soluble molybdate oxyanion ( $MoO_4^{2-}$ ), while the  $MoO_4^{2-}$  can be converted to thiomolybdates in euxinic conditions. It has been previously shown that thiomolybdates can be adsorbed onto humic substances and captured by Mn-Fe oxyhydroxides at the sediment surface [14,52,53]. Hence, the Mo-U covariance can be an indication of the paleo-redox conditions [48,52,54]. The enrichment factor (EF) for Mo and U were calculated using the equation  $EF = [(X/Al)_{sample}/(X/Al)_{PAAS}]$ , where X and Al represent the weight concentrations of elements X and Al, respectively. A plot of  $Mo_{EF}$  versus  $U_{EF}$  is presented in Table 5 and Figure 6. The plot shows that Niutitang samples were deposited in sulfidic/euxinic waters with higher EFs in Mo ( $EF > 10$ ) compared to U, while the  $Mo_{EF}$  versus  $U_{EF}$  plot also indicates that paleo-redox conditions went from anoxic in the Wufeng Formation to oxic in the upper Longmaxi Formation.

Basinal water mass restriction is correlated to paleo-redox condition [55], and it is mainly controlled by changes in sea level [56]. In a restricted sea, the Mo (ppm)/TOC (%) ratio in sediments decreases as the restriction increases, due to the low resupply rate of Mo in an aqueous medium [14]. In contrast, the ratio is higher in open marine sediments. This makes the Mo (ppm) to TOC ratio a useful tool in classifying paleo-hydrographic conditions. As shown in Figure 6b, the samples from the Niutitang and Wufeng formations were deposited in a moderately restricted basin. The ratio in the Longmaxi samples is lower than the Black Sea (~4.5), suggesting a strongly restricted condition with reducing sea level during this geological period.

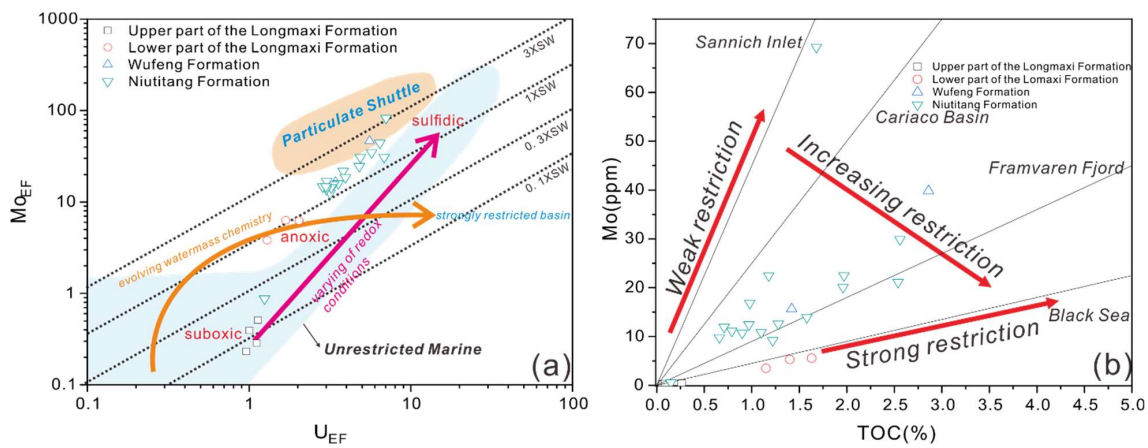


**Figure 6.** (a)  $Mo_{EF}$  versus  $U_{EF}$  in samples from the Wufeng-Longmaxi and the Niutitang Formations. The post-Archean average shale (PAAS) composition data used in this study are from Taylor and McLennan (1985) [33]. The interpretation lines are from Algeo and Tribovillard (2009) [52] and Tribovillard et al., (2012) [55]; (b) Mo (ppm) versus TOC (%) in samples from the Wufeng-Longmaxi and the Niutitang formations. The interpretation lines are from Algeo and Lyons (2006) [57] and Tribovillard et al. (2012) [55].

#### 5.4. Paleoproductivity

Primary paleo-productivity presents the total amount of organic matter produced per unit time and area [58], and hence good source rocks were deposited in areas of basins with elevated primary paleo-productivity [59,60]. Phosphorus (P) is a crucial nutritional element that is found in the skeleton [14,61]. P can exist as both dissolved and precipitated phases in seawater [62]. Sources of P can be divided into detrital and organic. Since the concentration of detrital P is usually very low, total P may serve as a proxy to estimate paleo-productivity [63].  $P_2O_5$  (%) and Ti (ppm) show no positive correlation in the samples of this study (Figure 7), indicating that P is of organic origin and can be used as a paleo-productivity proxy. A  $P/Ti$  ratio less than 0.34 reveals low paleo-productivity, and  $0.34 < P/Ti < 0.79$  and  $P/Ti > 0.79$  indicate medium and high paleo-productivities, respectively [64]. The  $P/Ti$  ratio in Niutitang shale ranges from 0.17 to 0.47 with an average of 0.22, while the average  $P/Ti$  ratio in Wufeng-Longmaxi shale is 0.11. Hence, the Wufeng-Longmaxi and Niutitang formations are characterized by low paleo-productivity. In addition, Wufeng-Longmaxi shale possess a lower paleo-productivity compared to the Niutitang shale in the study area (Table 5).

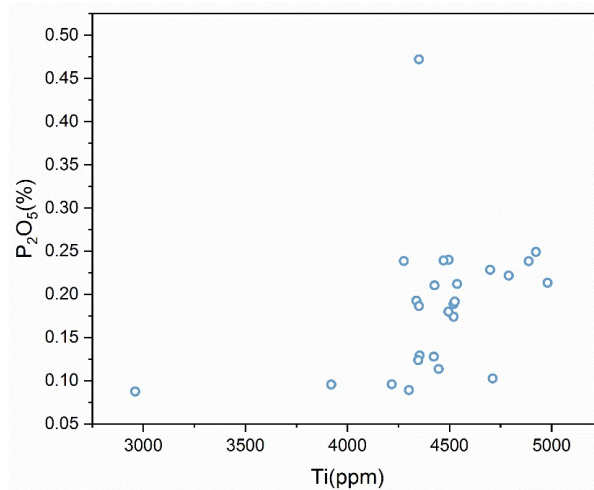


**Figure 7.** Relationship between  $P_2O_5$  (%) and Ti (ppm) in the samples.

### 5.5. Influence of Deposition Conditions on Organic Matter Enrichment

Total organic carbon (TOC) contents represent the amount of organic carbon, and it could be utilized to evaluate the richness of organic carbon and reveal hydrocarbon generation potential for hydrocarbon source rock [65]. The enrichment of organic matter in sediment is a complex process that is controlled by the input and preservation of organic matter [49], as well as its dilution by clastic input. Trends of TOC content and paleodeposition-related inorganic geochemical parameters with depth, in the samples, are shown in Figure 8. The relationship between different inorganic geochemical indicators and TOC contents are presented in Figure 9.

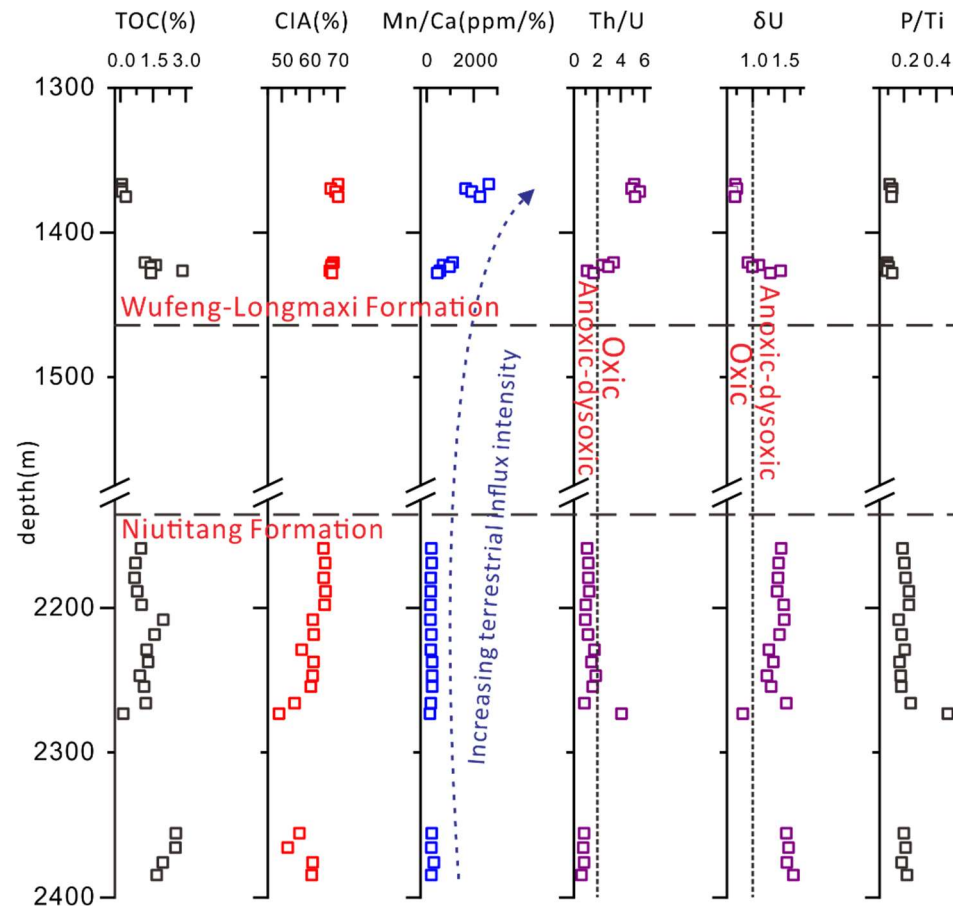


**Figure 8.** Trends of TOC content and paleodeposition-related inorganic geochemical parameters with depth.

A fair negative correlation can be observed in CIA and TOC content in the Wufeng-Longmaxi shale ( $R^2 = 0.49$ ), whereas it shows a poor correlation in the Niutitang samples (Figure 9a). Mn/Ca ratios are negatively related to TOC content for the Wufeng-Longmaxi samples ( $R^2 = 0.72$ ), while no clear relationship can be observed in the Niutitang samples (Figure 9b), indicating that the high terrestrial influx intensity in the Wufeng-Longmaxi samples diluted the TOC content and resulted in a negative correlation between Mn/Ca ratio and TOC content. In contrast, the terrestrial influx intensity for the Niutitang samples is low and had a minor effect on diluting TOC content. The regression analyses of Th/U,  $\delta U$ , and  $MO_{EF}$  with TOC contents are presented in Figure 9c–e. The results reveal a clear correlation between the redox parameters with TOC contents, suggesting anoxic conditions which helped with preservation of the organic matters. The study also found a positive relationship between P/Al and TOC content in the Wufeng-Longmaxi shale (Figure 9f). In addition, the correlation of P/Ti and TOC content is less ( $R^2 = 0.24$ ) in the Niutitang samples compared to the Wufeng-Longmaxi samples ( $R^2 = 0.46$ ).

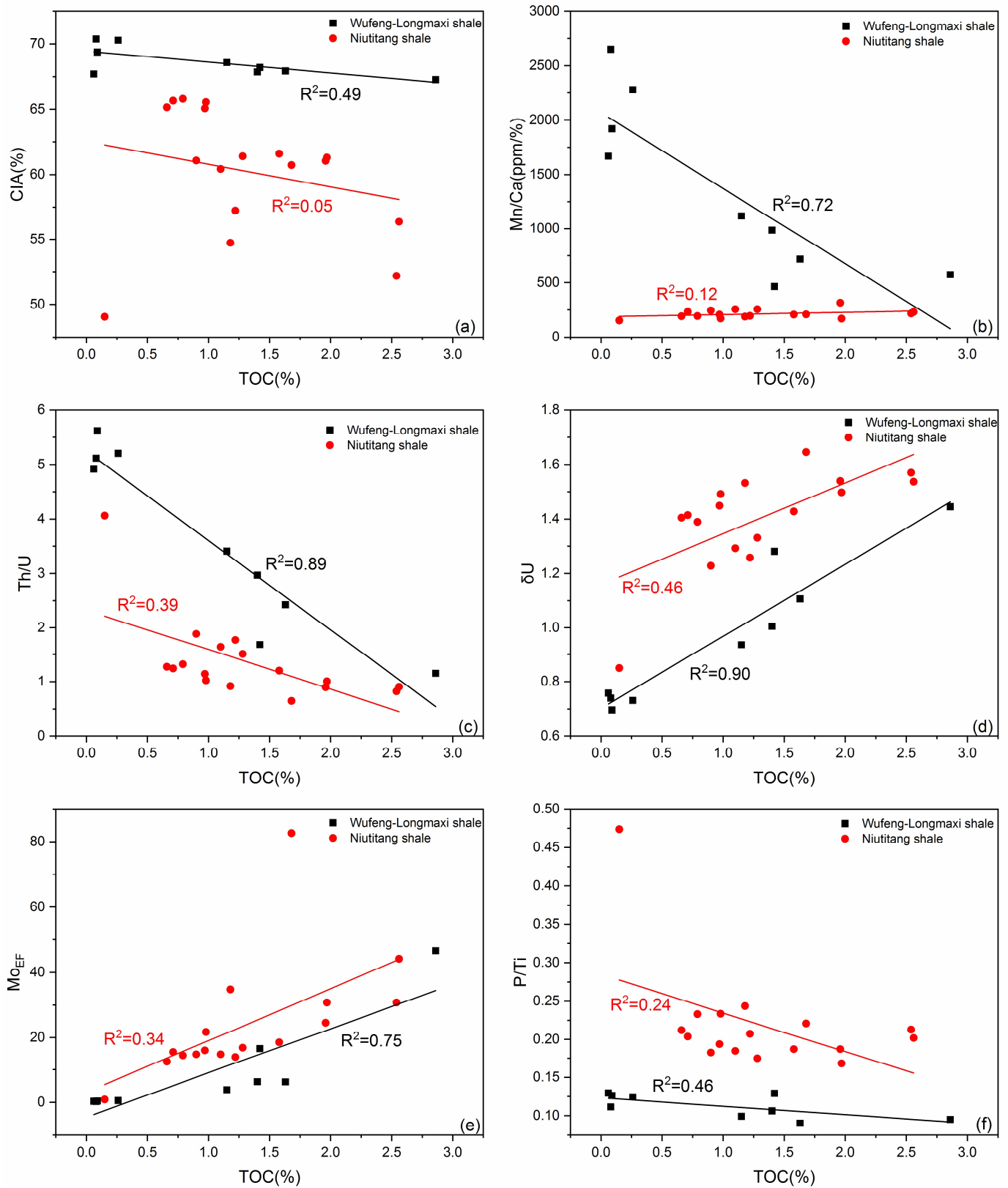


**Figure 9.** The relationship between different inorganic geochemical proxies and TOC contents.

### 5.6. Depositional and Organic Enrichment Models

Organic enrichment models mainly include preservation, production, and co-action models [66]. Cd/Mo and Co (ppm)  $\times$  Mn (%) proxies have been proposed and applied to determine

the dominant factor that impacts organic matter enrichment [66]. The results presented in Figure 10 indicate that the samples in the study well were mainly deposited in a restricted condition, based on Mo/TOC ratios. The Cd/Mn ratio reveals that organic matter enrichment of the Niutitang samples is mainly driven by preservation rather than productivity, while the dominating driving factor is the opposite for the Wufeng-Longmaxi samples.

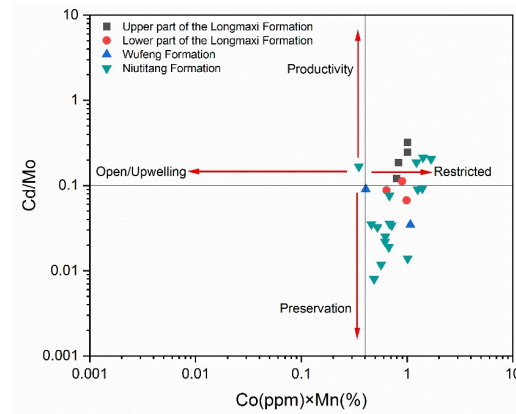


**Figure 10.** Cd/Mo versus Co (ppm) × Mn (%) for samples. The interpretation polygons are from Sweere et al. (2016) [66].

The Niutitang Formation was deposited in a moderately restricted basin with a eu-xinic reducing environment. This environment is considered to be the most suitable for preservation of organic matter (Figure 11a). The Wufeng Formation had similar reducing conditions and water mass restrictions to the Niutitang Formation (Figure 11b), but with increasing terrestrial influx intensity. As the water level decreased in the Longmaxi Formation, the terrestrial Influx steadily increased and diluted the richness of organic carbon. The hydrographic condition gradually became strongly restricted and the water environment shifted to dysoxic-oxic conditions due to a decrease in sea level, indicating that the paleo-productivity may have had a more significant impact on the organic matter enrichment compared to the paleo-redox condition (Figure 11c).

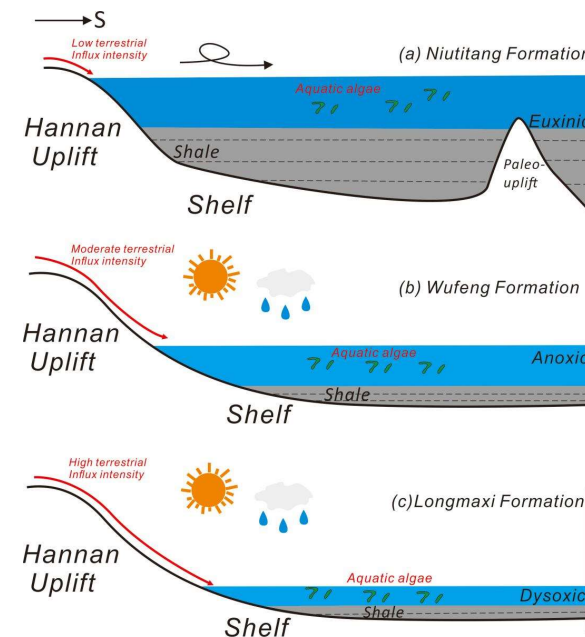


**Figure 11.** Organic matter enrichment model of shale from the Niutitang Formation (a), Wufeng Formation (b) and Longmaxi Formation (c).

## 6. Conclusions

The main conclusions from this study of the depositional environment and organic matter enrichment in Lower Paleozoic shale samples from the northeastern margin of the Yangtze Platform are as follows:

- (1) Warm and humid conditions existed for deposition of the Wufeng-Longmaxi samples. In contrast, palaeoclimatic condition indicators suggest cold and arid conditions in the Niutitang samples.
- (2) The terrestrial influx intensity in the Niutitang samples was relatively low. However, the terrestrial influx rate increased in the Wufeng and Longmaxi samples.
- (3) Parameters that measure palaeoredox conditions indicate an anoxic environment in the Niutitang, Wufeng and Lower Longmaxi samples. In contrast, the paleo-redox conditions were more oxic during the sedimentation of the Upper Longmaxi samples.
- (4) The P/Ti ratio reveals a low paleo-productivity for the Wufeng-Longmaxi and the Niutitang samples. Additionally, Wufeng-Longmaxi samples possess a lower paleo-productivity compared to the Niutitang samples in the well.
- (5) An obvious difference exists in the organic matter enrichment of the shale samples from different formations. The organic matter enrichment for samples in this study can be jointly influenced by paleo-redox conditions and paleo-productivity. Organic matter enrichment of the Niutitang shale is mainly driven by preservation rather than productivity. The dominant driving factor is the opposite for the Wufeng-Longmaxi shale.

**Author Contributions:** Methodology, P.L.; Investigation, P.L.; Writing—original draft, P.L.; Writing—review & editing, C.L. and R.G.; Funding acquisition, C.L. and R.G. All authors have read and agreed to the published version of the manuscript.

**Funding:** This study was financially supported by the “100-Talent” program from Chinese Academy of Sciences and the Postdoctoral Science Foundation of China (No. 2022MD713802).

**Institutional Review Board Statement:** Not applicable.

**Informed Consent Statement:** Not applicable.

**Data Availability Statement:** The data presented in this study are available on request from the corresponding author.

**Acknowledgments:** We would like to thank the reviewers for their valuable comments to improve the quality of the paper.

**Conflicts of Interest:** The authors declare no conflict of interest.

## References

1. Dong, D.; Shi, Z.; Guan, Q.; Jiang, S.; Zhang, M.; Zhang, C.; Wang, S.; Sun, S.; Yu, R.; Liu, D.; et al. Progress, challenges and prospects of shale gas exploration in the Wufeng–Longmaxi reservoirs in the Sichuan Basin. *Nat. Gas Ind. B* **2018**, *5*, 415–424. [[CrossRef](#)]
2. Zou, C.; Dong, D.; Wang, S.; Li, J.; Li, X.; Wang, Y.; Li, D.; Cheng, K. Geological characteristics and resource potential of shale gas in China. *Pet. Explor. Dev.* **2010**, *37*, 641–653. [[CrossRef](#)]
3. Guo, T. The Fuling Shale Gas Field—A highly productive Silurian gas shale with high thermal maturity and complex evolution history, southeastern Sichuan Basin, China. *Interpretation* **2015**, *3*, SJ25–SJ34. [[CrossRef](#)]
4. Chen, X.; Bao, S.; Zhai, G.; Zhou, Z.; Tong, C.; Wang, C. The discovery of shale gas within Lower Cambrian marine facies at Shan Nandi-1 well on the margin of Hannan palaeoplift. *China Geol.* **2018**, *45*, 412–413.
5. Jarvie, D.M.; Hill, R.J.; Ruble, T.E.; Pollastro, R.M. Unconventional shale-gas systems: The Mississippian Barnett Shale of north-central Texas as one model for thermogenic shale-gas assessment. *AAPG Bull.* **2007**, *91*, 475–499. [[CrossRef](#)]
6. Tissot, B.; Durand, B.; Espitalie, J.; Combaz, A. Influence of nature and diagenesis of organic matter in formation of petroleum. *AAPG Bull.* **1974**, *58*, 499–506.
7. Wang, Y.; Zhu, Y.; Liu, S.; Zhang, R. Methane adsorption measurements and modeling for organic-rich marine shale samples. *Fuel* **2016**, *172*, 301–309. [[CrossRef](#)]
8. Wu, Y.; Fan, T.; Jiang, S.; Yang, X.; Ding, H.; Meng, M.; Wei, D. Methane Adsorption Capacities of the Lower Paleozoic Marine Shales in the Yangtze Platform, South China. *Energy Fuels* **2015**, *29*, 4160–4167. [[CrossRef](#)]

9. Zou, J.; Rezaee, R.; Xie, Q.; You, L.; Liu, K.; Saeedi, A. Investigation of moisture effect on methane adsorption capacity of shale samples. *Fuel* **2018**, *232*, 323–332. [[CrossRef](#)]
10. Cox, G.M.; Jarrett, A.; Edwards, D.; Crockford, P.W.; Halverson, G.P.; Collins, A.S.; Poirier, A.; Li, Z.-X. Basin redox and primary productivity within the Mesoproterozoic Roper Seaway. *Chem. Geol.* **2016**, *440*, 101–114. [[CrossRef](#)]
11. Li, Y.; Liu, W.; Liu, P.; Luo, H.; Wang, X.; Zhang, D.; Yuan, Y. Paleoenvironment and Organic Matter Enrichment of the Middle Ordovician Marine Carbonates in the Ordos Basin of China: Evidence from Element Geochemistry. *ACS Earth Space Chem.* **2022**, *6*, 44–55. [[CrossRef](#)]
12. Mohialdeen, I.M.J.; Hakimi, M.H. Geochemical characterisation of Tithonian–Berriasian Chia Gara organic-rich rocks in northern Iraq with an emphasis on organic matter enrichment and the relationship to the bioproductivity and anoxia conditions. *J. Asian Earth Sci.* **2016**, *116*, 181–197. [[CrossRef](#)]
13. Schmid, S.; Kunzmann, M.; Pagès, A. Inorganic geochemical evaluation of hydrocarbon source rock potential of Neoproterozoic strata in the Amadeus Basin, Australia. *Mar. Pet. Geol.* **2017**, *86*, 1092–1105. [[CrossRef](#)]
14. Tribouvillard, N.; Algeo, T.J.; Lyons, T.; Riboulleau, A. Trace metals as paleoredox and paleoproductivity proxies: An update. *Chem. Geol.* **2006**, *232*, 12–32. [[CrossRef](#)]
15. Choi, J.H.; Hariya, Y. Geochemistry and depositional environment of Mn oxide deposits in the Tokoro Belt, northeastern Hokkaido, Japan. *Econ. Geol.* **1992**, *87*, 1265–1274. [[CrossRef](#)]
16. Li, Y.; Zhang, T.; Ellis, G.S.; Shao, D. Depositional environment and organic matter accumulation of Upper Ordovician–Lower Silurian marine shale in the Upper Yangtze Platform, South China. *Palaeogeogr. Palaeoclimatol. Palaeoecol.* **2017**, *466*, 252–264. [[CrossRef](#)]
17. Rimmer, S.M. Geochemical paleoredox indicators in Devonian–Mississippian black shales, Central Appalachian Basin (USA). *Chem. Geol.* **2004**, *206*, 373–391. [[CrossRef](#)]
18. Pan, S.; Liao, Y.; Jiang, B.; Wan, Z.; Wang, F. Impact of natural weathering on source rocks: Organic and inorganic geochemical evidence from the Triassic Chang 7 outcrop profile in Tongchuan of the Southern Ordos Basin (China). *Int. J. Coal Geol.* **2022**, *263*, 104119. [[CrossRef](#)]
19. Liu, Z.; Yan, D.; Du, X.; Li, S. Organic matter accumulation of the early Cambrian black shales on the flank of Micangshan-Hannan Uplift, northern upper Yangtze Block, South China. *J. Pet. Sci. Eng.* **2021**, *200*, 108378. [[CrossRef](#)]
20. Chang, Y.; Xu, C.H.; Reiners, P.W. The exhumation evolution of the Micang Shan-Hannan uplift since Cretaceous: Evidence from apatite (U-Th)/He dating. *Acta Geophys. Sin.* **2010**, *53*, 912–919.
21. Chen, X.; Guo, T.; Shi, D.; Hou, Q.; Wang, C. Pore structure characteristics and adsorption capacity of Niutitang Formation shale in southern Shaanxi. *Lithol. Reserv* **2019**, *31*, 52–60.
22. Tian, T.; Yang, P.; Ren, Z.; Fu, D.; Zhou, S.; Yang, F.; Li, J. Hydrocarbon migration and accumulation in the Lower Cambrian to Neoproterozoic reservoirs in the Micangshan tectonic zone, China: New evidence of fluid inclusions. *Energy Rep.* **2020**, *6*, 721–733. [[CrossRef](#)]
23. Zhang, Y.; Jia, X.; Wang, Z. Palaeogeography and provenance analysis of Early Cambrian Xiannüdong Formation in the Micangshan area. *Acta Geol. Sin.* **2019**, *93*, 2904–2920.
24. Liu, W.; Yang, X.; Shu, S.; Liu, L.; Yuan, S. Precambrian Basement and Late Paleoproterozoic to Mesoproterozoic Tectonic Evolution of the SW Yangtze Block, South China: Constraints from Zircon U–Pb Dating and Hf Isotopes. *Minerals* **2018**, *8*, 333. [[CrossRef](#)]
25. Ma, R.; Xiao, Y.; Wei, X.; He, Z.; Li, Y. The magmatic activity and tectonic evolution in the micangshan area, china. *J. Mineral. Petrol.* **1997**, *17*, 76–82.
26. Li, Y.; Xiong, X.; Feng, Y. Mesozoic uplift of the Dabashan and Micangshan-Hannan Dome in the South Qinling orogenic belt. *Sci. China Earth Sci.* **2022**, *65*, 426–436. [[CrossRef](#)]
27. Tian, T.; Zhou, S.; Fu, D.; Yang, F.; Li, J. Calculation of the original abundance of organic matter at high-over maturity: A case study of the Lower Cambrian Niutitang shale in the Micangshan-Hannan Uplift, SW China. *J. Pet. Sci. Eng.* **2019**, *179*, 645–654. [[CrossRef](#)]
28. Tuo, J.; Wu, C.; Zhang, M. Organic matter properties and shale gas potential of Paleozoic shales in Sichuan Basin, China. *J. Nat. Gas Sci. Eng.* **2016**, *28*, 434–446. [[CrossRef](#)]
29. Wu, J.; Liang, C.; Jiang, Z.; Zhang, C. Shale reservoir characterization and control factors on gas accumulation of the Lower Cambrian Niutitang shale, Sichuan Basin, South China. *Geol. J.* **2019**, *54*, 1604–1616. [[CrossRef](#)]
30. Fan, J.; Melchin, M.J.; Chen, X.; Wang, Y.; Zhang, Y.; Chen, Q.; Chi, Z.; Chen, F. Biostratigraphy and geography of the Ordovician–Silurian Lungmachi black shales in South China. *Sci. China Earth Sci.* **2011**, *54*, 1854. [[CrossRef](#)]
31. Xiao, B.; Xiong, L.; Zhao, Z.; Fu, X. Sedimentary tectonic pattern of Wufeng and Longmaxi Formations in the northern margin of Sichuan Basin, South China. *Int. Geol. Rev.* **2022**, *64*, 2166–2185. [[CrossRef](#)]
32. McLennan, S.M. Rare earth elements in sedimentary rocks; influence of provenance and sedimentary processes. *Rev. Mineral. Geochem.* **1989**, *21*, 169–200.
33. Taylor, S.R.; McLennan, S.M. *The Continental Crust: Its Composition and Evolution*; Blackwell Scientific Pub.: Palo Alto, CA, USA, 1985.
34. McLennan, S.M.; Hemming, S.R.; Taylor, S.R.; Eriksson, K.A. Early Proterozoic crustal evolution: Geochemical and NdPb isotopic evidence from metasedimentary rocks, southwestern North America. *Geochim. Cosmochim. Acta* **1995**, *59*, 1153–1177. [[CrossRef](#)]
35. Nesbitt, H.W.; Young, G.M. Early Proterozoic climates and plate motions inferred from major element chemistry of lutites. *Nature* **1982**, *299*, 715–717. [[CrossRef](#)]

36. McLennan, S.M. Weathering and Global Denudation. *J. Geol.* **1993**, *101*, 295–303. [[CrossRef](#)]
37. Fedo, C.M.; Wayne Nesbitt, H.; Young, G.M. Unraveling the effects of potassium metasomatism in sedimentary rocks and paleosols, with implications for paleoweathering conditions and provenance. *Geology* **1995**, *23*, 921–924. [[CrossRef](#)]
38. Tao, S.; Xu, Y.; Tang, D.; Xu, H.; Li, S.; Chen, S.; Liu, W.; Cui, Y.; Gou, M. Geochemistry of the Shitoumei oil shale in the Santanghu Basin, Northwest China: Implications for paleoclimate conditions, weathering, provenance and tectonic setting. *Int. J. Coal Geol.* **2017**, *184*, 42–56. [[CrossRef](#)]
39. Goodarzi, F. Comparison of the geochemistry of lacustrine oil shales of Mississippian age from Nova Scotia and New Brunswick, Canada. *Int. J. Coal Geol.* **2020**, *220*, 103398. [[CrossRef](#)]
40. Goodarzi, F.; Goodarzi, N.N.; Malachowska, A. Elemental composition, environment of deposition of the lower Carboniferous Emma Fiord formation oil shale in Arctic Canada. *Int. J. Coal Geol.* **2021**, *244*, 103715. [[CrossRef](#)]
41. Hayashi, K.-I.; Fujisawa, H.; Holland, H.D.; Ohmoto, H. Geochemistry of ~1.9 Ga sedimentary rocks from northeastern Labrador, Canada. *Geochim. Cosmochim. Acta* **1997**, *61*, 4115–4137. [[CrossRef](#)]
42. Li, Y.; Sun, P.; Liu, Z.; Yao, S.; Xu, Y.; Liu, R.; Li, Y. Geochemistry of the Permian Oil Shale in the Northern Bogda Mountain, Junggar Basin, Northwest China: Implications for Weathering, Provenance, and Tectonic Setting. *ACS Earth Space Chem.* **2020**, *4*, 1332–1348. [[CrossRef](#)]
43. Yang, B.; Hu, B.; Bao, Z.; Zhang, Z. REE geochemical characteristics and depositional environment of the black shale-hosted Baiguoyuan Ag-V deposit in Xingshan, Hubei Province, China. *J. Rare Earths* **2011**, *29*, 499–506. [[CrossRef](#)]
44. Zhao, Z.H. *Trace Elements Geochemistry*, 2nd ed.; Science Press: Beijing, China, 2016.
45. Roser, B.P.; Korsch, R.J. Determination of Tectonic Setting of Sandstone-Mudstone Suites Using SiO<sub>2</sub> Content and K<sub>2</sub>O/Na<sub>2</sub>O Ratio. *J. Geol.* **1986**, *94*, 635–650. [[CrossRef](#)]
46. Hatch, J.R.; Leventhal, J.S. Relationship between inferred redox potential of the depositional environment and geochemistry of the Upper Pennsylvanian (Missourian) Stark Shale Member of the Dennis Limestone, Wabaunsee County, Kansas, U.S.A. *Chem. Geol.* **1992**, *99*, 65–82. [[CrossRef](#)]
47. Jones, B.; Manning, D.A.C. Comparison of geochemical indices used for the interpretation of palaeoredox conditions in ancient mudstones. *Chem. Geol.* **1994**, *111*, 111–129. [[CrossRef](#)]
48. Wei, Y.; Li, X.; Zhang, R.; Li, X.; Lu, S.; Qiu, Y.; Jiang, T.; Gao, Y.; Zhao, T.; Song, Z.; et al. Influence of a Paleosedimentary Environment on Shale Oil Enrichment: A Case Study on the Shahejie Formation of Raoyang Sag, Bohai Bay Basin, China. *Front. Earth Sci.* **2021**, *9*, 736054. [[CrossRef](#)]
49. Zhao, B.; Li, R.; Qin, X.; Wang, N.; Zhou, W.; Khaled, A.; Zhao, D.; Zhang, Y.; Wu, X.; Liu, Q. Geochemical characteristics and mechanism of organic matter accumulation of marine-continental transitional shale of the lower permian Shanxi Formation, southeastern Ordos Basin, north China. *J. Pet. Sci. Eng.* **2021**, *205*, 108815. [[CrossRef](#)]
50. Kimura, H.; Watanabe, Y. Oceanic anoxia at the Precambrian-Cambrian boundary. *Geology* **2001**, *29*, 995–998. [[CrossRef](#)]
51. Wignall, P.B.; Twitchett, R.J. Oceanic Anoxia and the End Permian Mass Extinction. *Science* **1996**, *272*, 1155–1158. [[CrossRef](#)]
52. Algeo, T.J.; Tribovillard, N. Environmental analysis of paleoceanographic systems based on molybdenum-uranium covariation. *Chem. Geol.* **2009**, *268*, 211–225. [[CrossRef](#)]
53. Zheng, Y.; Anderson, R.F.; van Geen, A.; Kuwabara, J. Authigenic molybdenum formation in marine sediments: A link to pore water sulfide in the Santa Barbara Basin. *Geochim. Cosmochim. Acta* **2000**, *64*, 4165–4178. [[CrossRef](#)]
54. Wang, C.; Wang, Q.; Chen, G.; He, L.; Xu, Y.; Chen, L.; Chen, D. Petrographic and geochemical characteristics of the lacustrine black shales from the Upper Triassic Yanchang Formation of the Ordos Basin, China: Implications for the organic matter accumulation. *Mar. Pet. Geol.* **2017**, *86*, 52–65. [[CrossRef](#)]
55. Tribovillard, N.; Algeo, T.J.; Baudin, F.; Riboulleau, A. Analysis of marine environmental conditions based on molybdenum-uranium covariation—Applications to Mesozoic paleoceanography. *Chem. Geol.* **2012**, *324–325*, 46–58. [[CrossRef](#)]
56. Wu, Y.; Liu, C.; Liu, Y.; Gong, H.; Awan, R.S.; Li, G.; Zang, Q. Geochemical characteristics and the organic matter enrichment of the Upper Ordovician Tanjianshan Group, Qaidam Basin, China. *J. Pet. Sci. Eng.* **2022**, *208*, 109383. [[CrossRef](#)]
57. Algeo, T.J.; Lyons, T.W. Mo–total organic carbon covariation in modern anoxic marine environments: Implications for analysis of paleoredox and paleohydrographic conditions. *Paleoceanography* **2006**, *21*, PA1016. [[CrossRef](#)]
58. Gupta, L.P.; Kawahata, H. Downcore diagenetic changes in organic matter and implications for paleoproductivity estimates. *Glob. Planet. Chang.* **2006**, *53*, 122–136. [[CrossRef](#)]
59. Chen, G.; Gang, W.; Chang, X.; Wang, N.; Zhang, P.; Cao, Q.; Xu, J. Paleoproductivity of the Chang 7 unit in the Ordos Basin (North China) and its controlling factors. *Palaeogeogr. Palaeoclimatol. Palaeoecol.* **2020**, *551*, 109741. [[CrossRef](#)]
60. Xu, L.; Cheng, Y.; Zhang, J.; Liu, Y.; Yang, Y. Controls on the Organic Matter Accumulation of the Marine–Continental Transitional Shanxi Formation Shale in the Southeastern Ordos Basin. *ACS Omega* **2022**, *7*, 4317–4332. [[CrossRef](#)]
61. Redfield, A.C. The Biological Control of Chemical Factors in the Environment. *Am. Sci.* **1958**, *46*, 230A–221.
62. Paytan, A.; McLaughlin, K. The Oceanic Phosphorus Cycle. *Chem. Rev.* **2007**, *107*, 563–576. [[CrossRef](#)]
63. Schoepfer, S.D.; Shen, J.; Wei, H.; Tyson, R.V.; Ingall, E.; Algeo, T.J. Total organic carbon, organic phosphorus, and biogenic barium fluxes as proxies for paleomarine productivity. *Earth-Sci. Rev.* **2015**, *149*, 23–52. [[CrossRef](#)]
64. Yang, M.; Zuo, Y.; Fu, X.; Qiu, L.; Li, W.; Zhang, J.; Zheng, Z.; Zhang, J. Paleoenvironment of the Lower Ordovician Meitan Formation in the Sichuan Basin and Adjacent Areas, China. *Minerals* **2022**, *12*, 75. [[CrossRef](#)]

65. Dembicki, J.H. Chapter 3-Source Rock Evaluation. In *Practical Petroleum Geochemistry for Exploration and Production*; Dembicki, J.H., Ed.; Elsevier: Amsterdam, The Netherlands, 2017; pp. 61–133.
66. Sweere, T.; van den Boorn, S.; Dickson, A.J.; Reichart, G.-J. Definition of new trace-metal proxies for the controls on organic matter enrichment in marine sediments based on Mn, Co, Mo and Cd concentrations. *Chem. Geol.* **2016**, *441*, 235–245. [[CrossRef](#)]

**Disclaimer/Publisher's Note:** The statements, opinions and data contained in all publications are solely those of the individual author(s) and contributor(s) and not of MDPI and/or the editor(s). MDPI and/or the editor(s) disclaim responsibility for any injury to people or property resulting from any ideas, methods, instructions or products referred to in the content.